Journal of Medicinal Chemistry

Article

pubs.acs.org/jmc

Structure–Activity Relationships and Biological Characterization of a Novel, Potent, and Serum Stable C-X-C Chemokine Receptor Type 4 (CXCR4) Antagonist

Salvatore Di Maro,[†,⊥] Francesco Saverio Di Leva,[‡,⊥] Anna Maria Trotta,[§,⊥] Diego Brancaccio,[‡] Luigi Portella,[§] Michela Aurilio,[∥] Stefano Tomassi,[†] Anna Messere,[†] Deborah Sementa,[‡] Secondo Lastoria,[∥] Alfonso Carotenuto,[‡] Ettore Novellino,[‡] Stefania Scala,[*,§] and Luciana Marinelli[*,‡]

[†]DiSTABiF, University of Campania "Luigi Vanvitelli", Caserta 81100, Italy

[‡]Department of Pharmacy, University of Naples "Federico II", Via D. Montesano 49, 80131 Naples, Italy

[§]Functional Genomics Unit, Istituto Nazionale per lo Studio e la Cura dei Tumori "Fondazione Giovanni Pascale", IRCCS, Via M. Semmola 52, 80131 Naples, Italy

[∥]Nuclear Medicine Unit, Department of Diagnostic Imaging, Radiant and Metabolic Therapy, Istituto Nazionale per lo Studio e la Cura dei Tumori "Fondazione Giovanni Pascale", IRCCS, Via M. Semmola 52, 80131 Naples, Italy

Supporting Information

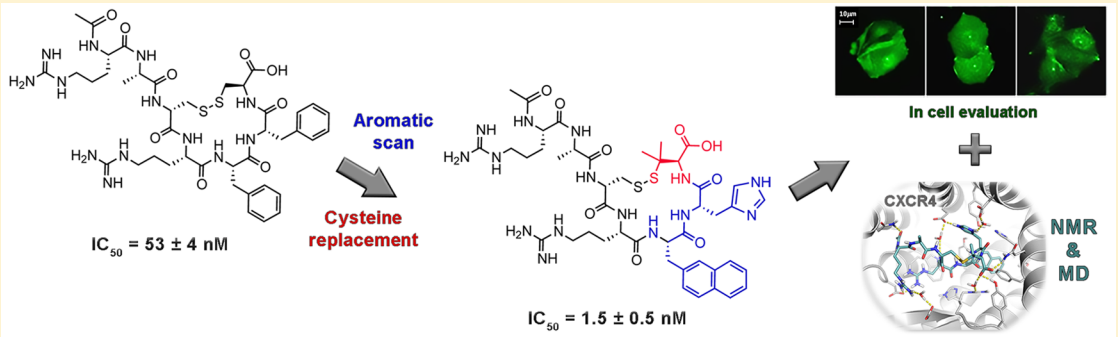

ABSTRACT: In our ongoing pursuit of CXCR4 antagonists as potential anticancer agents, we recently developed a potent, selective, and plasma stable peptide, Ac-Arg-Ala-[D-Cys-Arg-Phe-Phe-Cys]-COOH (**3**). Nevertheless, this compound was still not potent enough ($IC_{50} \approx 53$ nM) to enter preclinical studies. Thus, a lead-optimization campaign was here undertaken to further improve the binding affinity of **3** while preserving its selectivity and proteolytic stability. Specifically, extensive structure–activity relationships (SARs) investigations were carried out on both its aromatic and disulfide forming amino acids. One among the synthesized analogue, Ac-Arg-Ala-[D-Cys-Arg-Phe-His-Pen]-COOH (**19**), displayed subnanomolar affinity toward CXCR4, with a marked selectivity over CXCR3 and CXCR7. NMR and molecular modeling studies disclosed the molecular bases for the binding of **19** to CXCR4 and for its improved potency compared to the lead **3**. Finally, biological assays on specific cancer cell lines showed that **19** can impair CXCL12-mediated cell migration and CXCR4 internalization more efficiently than the clinically approved CXCR4 antagonist plerixafor.

INTRODUCTION

The chemokine receptor CXCR4 plays a central role in multiple physiological and pathological processes including tumor growth and metastasis.[1] CXCR4 is indeed highly expressed in more than 20 different solid and hematological cancer types, characterized by high aggressiveness, and eager to metastasize toward secondary organs where the endogenous CXCR4 ligand CXCL12/SDF-1α (stromal-cell derived factor 1α) is produced.[2] Emerging evidence demonstrates that primary tumor releases soluble factors able to remodel the microenvironment in secondary organs predisposing "premetastatic niches" where neoplastic cells will seed. CXCL12 plays a pivotal role in this process through the recruitment of bone marrow derived cells and neuthrophils.[3] In fact, the clinically approved CXCR4 antagonist plerixafor (**1**),[4] also known as AMD3100 (Chart 1), inhibits the tissue inhibitor of metalloproteinases (TIMP-1) that controls the liver premetastatic niches in colorectal cancer patients.[5] Along the same line, an AMD3100 analogue had been previously shown to modulate oncogenic mediators such as MMP2, GSK3, cMYC, AKT, and STAT3, inhibiting the formation of a cancer nurturing microenvironment and in turn metastasis.[6] Moreover, it is now well established that, besides being a fertile soil for cancer

Received: July 24, 2017
Published: November 10, 2017

DOI: 10.1021/acs.jmedchem.7b01062
J. Med. Chem. 2017, 60, 9641–9652

Chart 1. Chemical Structures of 1 (plerixafor) and 3

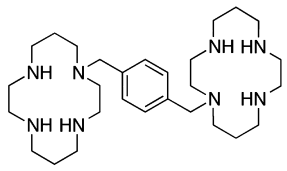

1

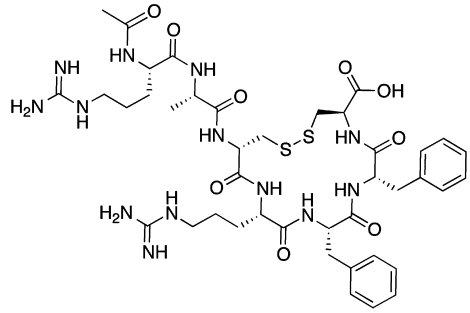

3

growth, the microenvironment can facilitate immune escape of tumor cells. In this perspective, the aberrant recruitment of CXCR4 expressing cells together with an increment of CXCL12 in stroma represent key events in metastasis process via both tumor-specific and T-cell based mechanisms. At this regard, improved efficacy of targeting immune checkpoints receptors (ICRs) was recently demonstrated by some of us through coupling of immune checkpoints inhibitors with CXCR4 antagonists such as **1**.[7] Moreover, interactions between stromal cells producing CXCL12 such as cancer-associated fibroblasts (CAFs) and neoplastic cells have been demonstrated to have an impact on metabolic reprogramming of cancer cells.[8] Also, recent evidence demonstrates that CXCL12 plays a role in promoting a glycolytic shift, known as the "Warburg" effect, in leukemic cells through the CXCR4/mTOR signaling axis. Notably, plerixafor administration in acute myeloid leukemia cells markedly reduces glucose uptake, mTOR activation, and consequently basal glycolysis and glycolytic capacity.[9] Besides plerixafor and plerixafor-like derivatives, a number of peptidic and nonpeptidic CXCR4 antagonist have been discovered so far.[10−17] Among these, prominent examples are the protein epitope mimetic POL5551,[10] the 14-mer peptides H-Arg-Arg-Nal-Cys-Tyr-Arg-Lys-D-Lys-Pro-Tyr-Arg-Cit-Cys-Arg-OH (T140),[11] and 4F-benzoyl-Arg-Arg-Nal-Cys-Tyr-Cit-Lys-D-Lys-Pro-Tyr-Arg-Cit-Cys-Arg-NH_2 (BKT140)[12] and their downsized cyclic derivatives such as cyclo[Arg^1-Arg^2-Nal^3-Gly^4-D-Tyr^5] (FC131),[13] as well as cyclo[Phe-Tyr-Lys(iPr)-D-Arg-2-Nal-Gly-D-Glu]-Lys(iPr)-NH_2 (LY2510924).[16] Also, several CXCR4-targeting probes for molecular imaging were developed.[18] Indeed, the in vivo assessment of CXCR4 expression can provide relevant information on tumor biology and identify patients eligible for CXCR4-targeted therapies. In this perspective, AMD derivatives have been investigated for ^{64}Cu-,[19] ^{18}F-,[20] and even ^{11}C-labeling.[21] Recently, a radiolabeled CXCR4-ligand ([^{68}Ga]pentixafor) for PET imaging has been successfully utilized in patients with hematologic and solid malignancies.[22] As a part of our continued effort to find effective CXCR4 antagonists,[15] starting from a CXCL12-mimetic cyclic peptide (H-Arg-Ala-[Cys-Arg-Phe-Phe-Cys]-COOH)[23] (**2**), we have recently reported the design and synthesis of a plasma stable CXCR4 peptide antagonist (Ac-Arg-Ala-[D-Cys-Arg-Phe-Phe-Cys]-COOH) (**3**) (Chart 1), which was able to selectively bind the receptor with an IC_{50} of 53 nM.[24] In spite of its promising pharmacological and pharmacokinetic profile, **3** was still not suited for comprehensive in vivo studies since a low nanomolar or picomolar IC_{50} is generally required for such investigations.

Therefore, a lead-optimization study was here undertaken to further improve the peptide binding potency, without affecting its stability in biological fluids, with the final aim to achieve an optimal CXCR4 response and minimize the potential side effects due to off-target interactions. To reach this goal, we have performed an extensive structure−activity relationship (SAR) study around both the overall cycle conformation and the two aromatic amino acids of **3**. The novel cyclic peptides were evaluated as CXCR4 antagonists through the inhibition of receptor binding of anti-CXCR4 PE-antibodies (clone 12G5), and for the most affine compound (**19**) the potency was further quantified through a iodine-125 CXCL12 competition test in human leukemic lymphoblast (CCRF-CEM cells). These assays showed that **19** is able to displace the labeled chemokine with an IC_{50} of 20 ± 2 nM, thus representing a new potent CXCR4 antagonist. The selectivity of action of **19** was then demonstrated through binding assays on CXCR3 and CXCR7 overexpressing cell lines. NMR and molecular modeling disclosed the molecular bases for the binding of **19** to CXCR4, also explaining the structure−activity relationships of all the other newly synthesized peptides. Finally, the biological efficacy of **19** was demonstrated through the evaluation of CXCL12-dependent cell migration and CXCL12-mediated CXCR4 internalization in specific cancer cell lines.

RESULTS AND DISCUSSION

Design. Our previous Ala-scan study on **3** pointed out that L-Arg at both the 1 and 4 positions and the two L-Phe at 5 and 6 positions were fundamental for the interaction with the CXCR4 receptor. In the attempt to improve the activity of **3**, a three-step structure−activity relationship study was designed. In the first step, we explored the cycle conformation of **3** by replacing either the L-Cys (position 7) or the D-Cys (position 3) or both with penicillamine (Pen) (compounds **4**−**6**). The most potent analogue (**4**) emerging from this first round of modifications entered the second phase of the study. In detail, the Phe residues at the 5 or 6 position were, one at a time, replaced by amino acids bearing smaller aromatic side chains, such as L-His (**7**, **13**), or bulkier side chains, such as L-1- and L-2-naphthylalanine (L-1-Nal, L-2-Nal) (**11**, **17** and **12**, **18**, respectively), or substituted on the phenyl ring with electron withdrawing (4-Cl and 4-NO_2) (**9**, **15** and **10**, **16**) or electron donor (4-OH) (**8**, **14**) groups. Finally, the most effective modifications (**4**, **12**, and **13**) were simultaneously applied into a single compound (**19**) to check whether their combination would result in a further increment of potency.

Chemistry. All the linear heptapeptides were assembled in solid phase by standard Fmoc/^{t}Bu protocol using 2-chlorotrityl resin as support in order to minimize the potential racemization of the first amino acid during the loading process.[25]

DOI: 10.1021/acs.jmedchem.7b01062
J. Med. Chem. 2017, 60, 9641−9652

Table 1. IC_{50} Values (Mean ± SD) for CXCR4 Antagonist Peptides Obtained Measuring the Inhibition of Receptor Binding of Anti-CXCR4 PE-Antibodies (Clone 12G5)

compd	sequence	IC_{50} (nM)
2	H-Arg-Ala-[Cys-Arg-Phe-Phe-Cys]-COOH	6200 ± 1300
3	Ac-Arg-Ala-[D-Cys-Arg-Phe-Phe-Cys]-COOH	53 ± 4
4	Ac-Arg-Ala-[D-Cys-Arg-Phe-Phe-**Pen**]-COOH	40 ± 10
5	Ac-Arg-Ala-[**D-Pen**-Arg-Phe-Phe-Cys]-COOH	>10000
6	Ac-Arg-Ala-[**D-Pen**-Arg-Phe-Phe-**Pen**]-COOH	1530 ± 40
7	Ac-Arg-Ala-[D-Cys-Arg-**His**-Phe-**Pen**]-COOH	>10000
8	Ac-Arg-Ala-[D-Cys-Arg-**Tyr**-Phe-**Pen**]-COOH	2140 ± 300
9	Ac-Arg-Ala-[D-Cys-Arg-(**4-Cl**)**Phe**-Phe-**Pen**]-COOH	70 ± 20
10	Ac-Arg-Ala-[D-Cys-Arg-(**4-NO_2**)**Phe**-Phe-**Pen**]-COOH	210 ± 70
11	Ac-Arg-Ala-[D-Cys-Arg-**1-Nal**-Phe-**Pen**]-COOH	3690 ± 1810
12	Ac-Arg-Ala-[D-Cys-Arg-**2-Nal**-Phe-**Pen**]-COOH	22 ± 2
13	Ac-Arg-Ala-[D-Cys-Arg-Phe-**His-Pen**]-COOH	6 ± 2
14	Ac-Arg-Ala-[D-Cys-Arg-Phe-**Tyr-Pen**]-COOH	360 ± 60
15	Ac-Arg-Ala-[D-Cys-Arg-Phe-(**4-Cl**)**Phe-Pen**]-COOH	1250 ± 630
16	Ac-Arg-Ala-[D-Cys-Arg-Phe-(**4-NO_2**)**Phe-Pen**]-COOH	>10000
17	Ac-Arg-Ala-[D-Cys-Arg-Phe-**1-Nal-Pen**]-COOH	180 ± 40
18	Ac-Arg-Ala-[D-Cys-Arg-Phe-**2-Nal-Pen**]-COOH	1800 ± 560
19	Ac-Arg-Ala-[D-Cys-Arg-**2-Nal-His-Pen**]-COOH	1.5 ± 0.5
1	AMD 3100	6 ± 4

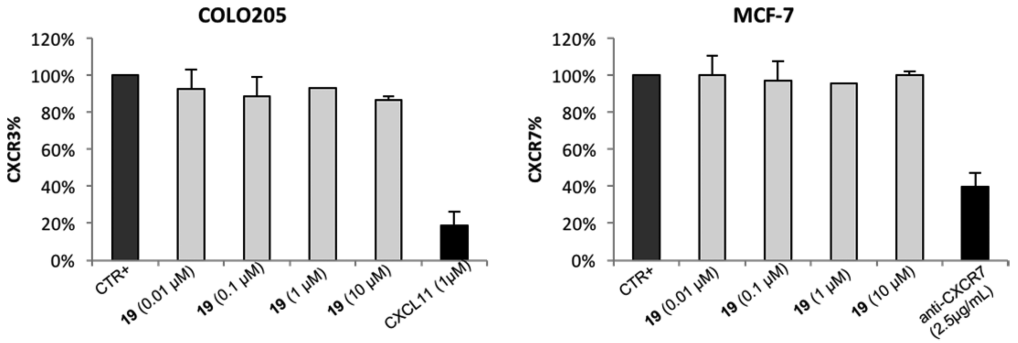

Figure 1. Binding of **19** to (A) COLO205 colon cancer cells, overexpressing CXCR3, and (B) MCF-7 breast cancer cell line, overexpressing CXCR7. The binding was evaluated through flow cytometry using anti-CXCR3 FITC-antibody and anti-CXCR7 APC-antibody. Data are presented as bar graph showing mean ± SD.

Unfortunately, the replacement of L-Cys (position 7) with a residue of L-Pen produced linear final products in substantial lower yield, when the first amino acid was loaded by classical reported protocol (15% L-Pen vs 60% L-Cys). In our opinion, the observed lack of synthetic efficiency was probably due to the more hindered side chain of penicillamine compared with cysteine. Thus, to increase the yield of the coupling of the first amino acid, we used an excess of resin (2 equiv) with respect to the latter. This strategy indeed provides a larger number of the chlorine reactive groups involved in the loading of the first amino acid. By using this alternative approach, we were able to increase the yield of the final linear compounds from 15% to about 55%. Once assembled on the solid support, all the linear heptapeptides were removed from the resin and the resulting free thiol groups were eventually oxidized using *N*-chlorosuccinimide to form the desired disulfide bridge.[26]

CXCR4 Binding Assays. All the peptides were preliminarily assessed against CXCR4 measuring their ability to inhibit receptor binding of anti-CXCR4 PE-conjugated antibody (clone 12G5) in CEM-CCRF human T leukemia cells that overexpress CXCR4.[27] First, we evaluated the effects of the replacement of D-Cys^3 and L-Cys^7 in the lead peptide **3** with D- and L-Pen, respectively.[28] As reported in Table 1, the latter modifications led to an enhancement of affinity toward CXCR4, with peptide **4** able to reduce the receptor/antibody interaction with an IC_{50} of 40 ± 10 nM. Conversely, the introduction of a D-Pen in place of D-Cys^3 (**5**) completely abolished the binding. Also, a dramatic lack of affinity was observed when both D- and L-Pen were simultaneously inserted at the 3 and 7 positions, respectively, with compound **6** showing an IC_{50} of about 1530 ± 40 nM. These results would thus indicate that the two methyl groups on the α-carbon of Pen modify the orientation of the pharmacophoric amino acid side chains, which is however favorable for the binding only in the case of L-Cys^7 substitution. Next, further structure−activity relationship studies were performed by replacing the two L-Phe residues of peptide **4**. Indeed, compound **7**, featuring L-His in place of Phe^5, turned out as totally inactive; conversely, **13**, obtained through the Phe^6/His substitution, showed a remarkably higher affinity for the receptor (IC_{50} = 6 ± 2 nM). Also, when either position 5 or position 6 was substituted with a L-Tyr residue (**8** and **14**), we observed a marked drop in affinity for the receptor if compared to peptide **4**. On the other hand, the introduction of a chlorine in para position of the Phe^5 and Phe^6 aromatic ring (**9**−**15**) produced diametrically opposite results. In particular, the presence of a (4-Cl)-L-Phe

DOI: 10.1021/acs.jmedchem.7b01062
J. Med. Chem. 2017, 60, 9641−9652

residue at the 5 position (**9**) was well tolerated, while the same group at the 6 position (**15**) dramatically reduced the affinity for the receptor. Negative results were also observed when we introduced alternative withdrawing groups such as a nitro group at the 5 (**10**, IC_{50} = 210 ± 70 nM) and 6 positions (**16**, IC_{50} > 10 000 nM). Next, the influence on peptide binding of bulkier side chain was investigated by inserting L-1- and L-2-Nal residues in place of Phe^5 and Phe^6. Among the resulting analogues, **11** and **17**, bearing L-1-Nal at 5 and 6 positions, respectively, and **18**, bearing L-2-Nal at the 6 position, showed reduced receptor binding potency if compared to peptide **4**. Conversely, peptide **12**, obtained through the replacement of Phe^5 with 2-Nal, was about 2 times more potent than **4** (IC_{50} = 22 ± 2 nM). Considering the good results achieved by introducing 2-Nal in place of Phe^5 and His in place of Phe^6, we decided to combine these two modifications in a unique compound, namely, **19**. Noteworthy, this peptide showed the ability to inhibit the receptor binding of PE-conjugated 12G5 anti-CXCR4 antibody in the low nanomolar range (IC_{50} = 1.5 ± 0.5 nM).

Binding Specificity. To demonstrate the specificity of **19** toward CXCR4 over other chemokine receptors, flow cytometry binding experiments were also conducted on the CXCR3-overexpressing COLO205 human colorectal cancer cell line and on MCF-7 human breast cancer cells which overexpress the CXCR7 receptor. Cells were incubated with **19**, and then the peptide ability to impair the binding of specific anti-CXCR3 (anti-CXCR3 FITC-antibody, R&D FAB160F clone 49801) and anti-CXCR7 (anti-CXCR7 APC-antibody, R&D FAB4227A clone 11G8) antibodies was evaluated. As shown in Figure 1, **19** was not able to affect the binding of the latter antibodies to their receptor counterpart, indicating that our peptide can bind neither CXCR3 nor CXCR7. These assays therefore demonstrate that similar to its parent peptide **3**,[24] **19** is a selective CXCR4 ligand.

^{125}I-CXCL12 Competition Binding Assay. The enhancement of affinity toward CXCR4 obtained with **19** was further quantified by investigating the capability of this peptide, in comparison with the lead **3**, to compete with the radiolabeled tracer ^{125}I-CXCL12.[29] Fixed amounts of the ^{125}I-labeled CXCL12 were incubated with CCRF-CEM cells in the presence of increasing concentrations of **3** or **19**. As shown in Figure 2, **19** can displace ^{125}I-labeled CXCL12 more efficiently than **3** (**19**, IC_{50} = 20 ± 2 nM vs **3**, IC_{50} = 338 ± 12 nM), showing a potency similar to other CXCR4 antagonists which are at different stages of development. In particular, the binding affinity of **19** is comparable to that of **1**, which is the only CXCR4 antagonist approved for stem cell mobilization.[30]

Cell Migration Assay. To functionally characterize the newly developed peptide **19**, we evaluated its effect on the CXCL12-mediated migration of CCRF-CEM cells in Transwell-based assays, including **1** as reference compound. These assays revealed that **19** can inhibit CCRF-CEM migration more efficiently than **1**, even at low nanomolar concentration (Figure 3A). Further experiments demonstrated that **19** can also impair the CXCL12-induced migration of other cancer cell lines such as the PES43 metastatic melanoma cells (Figure 3B), the HT29 and HCT116 human colon cancer cells (Figure 3C,D), and the A498 and SN12C human renal cancer cells (Figure 3E,F), in a concentration dependent manner, thus showing a comparable range of efficacy with the unique clinically approved CXCR4 antagonist **1**.

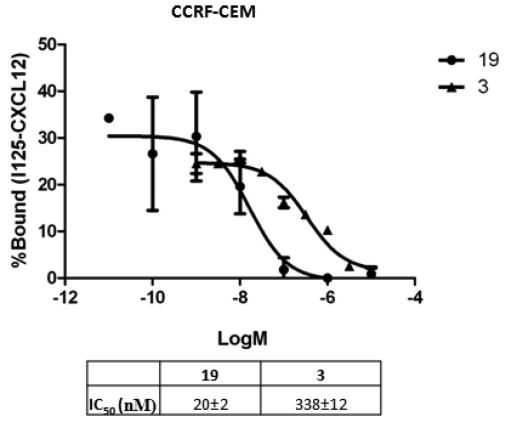

	19	3
IC_{50} (nM)	20±2	338±12

Figure 2. Competition binding assays of **19** with ^{125}I-CXCL12. Experiments were performed on CCRF-CEM cells. Cells were incubated with 60 pM ^{125}I-CXCL12 as tracer and increasing concentrations (from 10 pM to 10 μM) of either **3** or **19** as competitor. The binding curve was fitted to a one-site binding model. Results shown (mean ± SD) are the average of three experiments.

CXCR4 Internalization. Like other GPCR receptors, CXCR4 is rapidly internalized upon ligand binding and accumulates into endosomal vesicles.[31] Using CHO cells transfected with green fluorescent protein (GFP) tagged CXCR4, we analyzed the effect of the newly developed **19** in the receptor internalization process in comparison with **1**. Briefly, CHO-CXCR4-GFP cells were treated with **1** or **19**, and the CXCR4 receptor internalization process was studied from 30 min up to 24 h in the presence of the specific ligand CXCL12 (12.5 nM) by confocal microscopy. Upon ligand binding the GFP-CXCR4 receptor (in green, Figure 4) clearly accumulates into endosomal vesicles, identifiable as bright green spots in the cytoplasm (Figure 4B) as compared to untreated cells (Figure 4A); this effect was impaired by **19** (Figure 4C) but not by **1** (Figure 4D). Thus, **19**, different from **1**, is able to efficiently inhibit the CXCR4 internalization process. This effect is detectable from 30 min to 6 h after treatment, while it cannot be determined at 24 h.

Serum Stability. The early metabolic stability of **19** was assessed by incubating it and its unstable parent peptide **2** in 90% human serum at 37 °C according to a previously described protocol.[32] At several time intervals, aliquots of the mixture reaction were collected, treated with acetonitrile to precipitate the serum proteins, and analyzed by ESI-RP-HPLC. As shown in Figure 5, the reference peptide starts to be significantly degraded already after 15 min, when we could detect around 67% of intact compound and the formation of about 23% and 10% of the corresponding hexapeptide and pentapeptide metabolites, respectively. After 30 min, the reference sequence was fully converted into the corresponding cyclic pentapeptide metabolite H-[Cys-Arg-Phe-Phe-Cys]-COOH. In line with the results of our previous study, **19** was stable up to 120 min, confirming our observation that the introduction of the acetyl group at the N-terminal region was sufficient to preserve the peptide against human serum proteolytic degradation.

NMR Spectroscopy. NMR experiments were performed on the most active compound **19**. Complete ^{1}H NMR chemical shift assignments (Table S1 in Supporting Information) were performed according to the Wüthrich procedure.[33] DQF-COSY,[34] TOCSY,[35] and NOESY[36] experiments, with the support of the XEASY software package,[37] were carried out in

DOI: 10.1021/acs.jmedchem.7b01062
J. Med. Chem. 2017, 60, 9641−9652

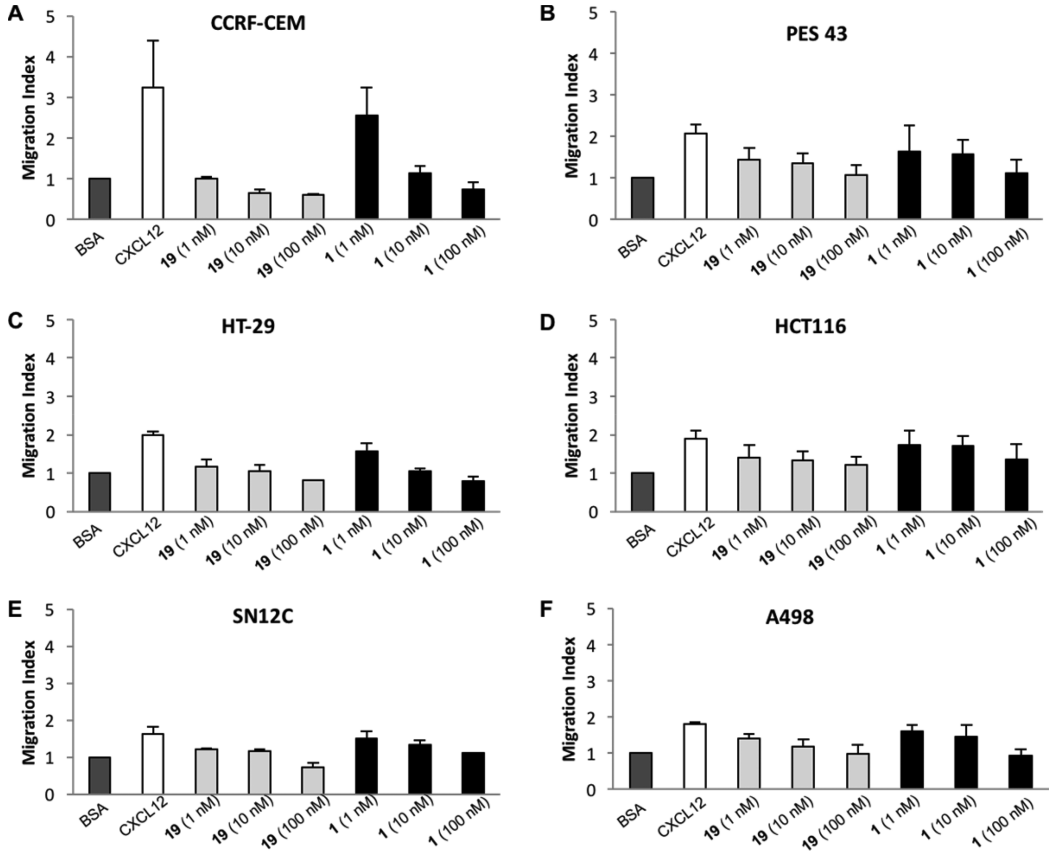

Figure 3. Comparative CXCL12-dependent cells migration experiments on **1** and **19**. Experiments were conducted on the CCRF-CEM (A), PES43 (B), HT29 (C), HCT116 (D), SN12C (E), and A498 (F) cell lines. Migrated cells on the lower surface were fixed, stained with H&E, and counted microscopically. The results are expressed as the migration index relative to migration in the presence of BSA alone. Data are presented as bar graph showing mean ± SD.

200 mM SDS micellar solution. The employment of SDS micelles to investigate the conformational properties is justified on the basis of their interaction with a membrane receptor. For peptides that bind membrane receptors, such as GPCR, the use of membrane mimetic solution is suggested, hypothesizing a membrane-assisted mechanism of interactions between the peptides and their receptors;[38] in fact, micelle solutions have been extensively used for peptide hormones conformational studies.[39] Many NMR parameters of **19** indicate a folded structure. In particular, NOE contacts between H_{α}-NH_{i+2} of Arg^1 and D-Cys^3 and NH-NH_{i+2} of D-Cys^3 and Nal^5 and between Arg^4 and His^6 indicated that folded structures span along the entire peptide sequence. The presence of those structures is confirmed by low values of the temperature coefficients of amide protons ($|\Delta\delta/\Delta T| < 4$ ppb/K) of D-Cys^3, His^6, and Pen^7 (Table S1). Upfield shifts of side chain protons of the Arg^4 and NOE contacts between Arg^4 and 2-Nal^5 and between 2-Nal^5 and His^6 point to a spatial proximity of these couples of side chains. Also Arg^1 and Ala^2 side chains show NOE interactions with 2-Nal^5 naphthyl moiety indicating that the exocyclic side chains are close to the endocyclic pharmacophoric triad formerly consisting of the Arg^4-Phe^5-Phe^6 sequence. NMR constraints from SDS micelle solution were used as the input data for a simulated annealing structure calculation (Table S2). An ensemble of well-defined structures was obtained (Figure 6A). Calculated structures satisfied the NMR-derived constraints (violations smaller than 0.20 Å). The 10 lowest energy structures for **19** showed a rmsd of 0.12 Å and a well-defined β-turn (type IV) along residues 4−7. Also the side chain positions are well-defined, in fact the all atom rmsd is only 0.64 Å. This structural stability is likely to contribute to the activity enhancement observed for **19** compared to **3** that was more flexible in the same experimental conditions.[24] A three-dimensional superposition of NMR-derived structures of **3** and **19** (Figure 6B) shows that both the cycle and the side chains are close in the space (rmsd between the two lowest energy conformers of **3** and **19** is only 0.79 Å when all the Cγ atoms are considered).

Molecular Modeling. To elucidate the binding mode of our newly synthesized peptides to CXCR4, molecular modeling studies were performed on the most potent compound of the series **19**. In analogy with our previous investigations on the lead peptide **3**,[24] standard docking algorithms were not able to predict reliable ligand binding poses; therefore, a more advanced computational approach was again employed. Specifically, we carried out extensive molecular dynamics (MD) simulations in explicit solvent and membrane on the **19**/CXCR4 complex that was obtained through a manual docking procedure (see the Experimental Section and the Supporting Information for details). According to MD results, the Arg^4, 2-Nal^5, and His^6 side chains of **19** deepen into the transmembrane (TM) bundle of CXCR4 (Figure 7A), occupying both the minor (TMS1; between TM1, TM2, TM3, and TM7) and the major pocket (TMS2; between TM3, TM4, TM5, TM6, and TM7)[40] of the ligand binding site. In detail, the Arg^4 guanidinium group establishes a tight salt bridge

DOI: 10.1021/acs.jmedchem.7b01062
J. Med. Chem. 2017, 60, 9641−9652

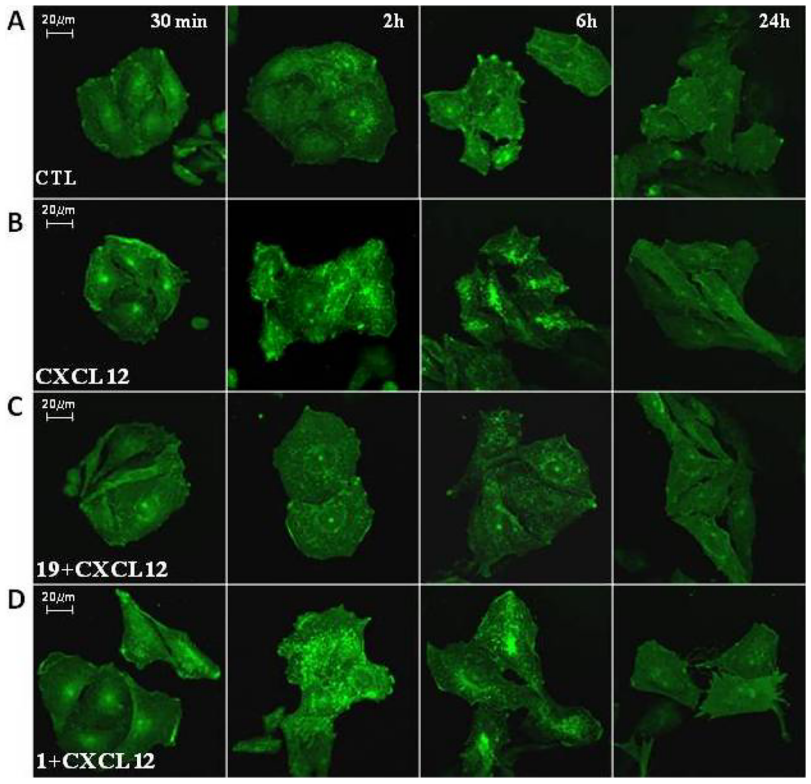

Figure 4. CXCR4 internalization was assessed in CHO-CXCR4-GFP cells in the presence of CXCL12 (12.5 nM), **19** (10 nM), and **1** (10 nM): (A) untreated cells; (B) cells treated with CXCL12 (12.5 nM); (C) cells treated with **19** (10 nM) and then stimulated with CXCL12 (12.5 nM); (D) cells treated with **1** (10 nM) and then stimulated with CXCL12 (12.5 nM).

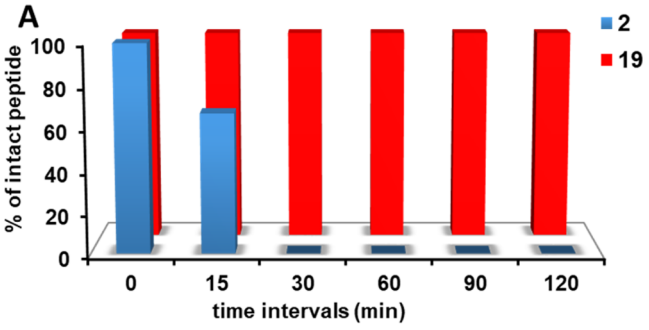

B

Time intervals (min)	2	2-R*	2-RA**	19
0	900.4 (100%)	788.3 (0%)	673.3 (0%)	1009.4 (100%)
15	900.4 (67%)	788.3 (23%)	673.3 (10%)	1009.4 (100%)
30	900.4 (0%)	788.3 (0%)	673.3 (100%)	1009.4 (100%)
60	900.4 (0%)	788.3 (0%)	673.3 (100%)	1009.4 (100%)
90	900.4 (0%)	788.3 (0%)	673.3 (100%)	1009.4 (100%)
120	900.4 (0%)	788.3 (0%)	673.3 (100%)	1009.4 (100%)

2-R*= H-Ala-[Cys-Arg-Phe-Phe-Cys]-COOH
2-RA*= H-[Cys-Arg-Phe-Phe-Cys]-COOH

Figure 5. (A) Stability of **2** and **19** at different intervals of incubation with 90% human serum. Relative concentrations of peptides were determined by integration of the A230 peaks from analytical HPLC. (B) ESI-MS characterizations of **2** and **19** at different intervals of incubation.

with the D97$^{2.63}$ carboxylate group and a cation−π interaction with W94$^{2.60}$, while the 2-Nal^{5} side chain extends into the aromatic cage defined by H113$^{3.29}$, Y116$^{3.32}$, Y121$^{3.37}$, F199$^{5.38}$, H203$^{5.42}$, and Y255$^{6.51}$, forming favorable contacts with the side chains of these residues together with a cation−π with the R188$^{45.52}$ guanidinium group. In the neighboring cleft the protonated His^{6} imidazole ring establishes a T-shaped stacking interaction with the Y255$^{6.51}$ phenol ring and, more interestingly, a salt bridge with the conserved E288$^{7.39}$ carboxylate group and a water mediated interaction with D262$^{6.58}$. Aside from the Arg^{4}, 2-Nal^{5}, and His^{6} triad, also the other peptide amino acids are involved in the binding of **19** to CXCR4. For instance, the Arg^{1} side chain, analogous to Arg^{4}, makes a salt bridge with the D97$^{2.63}$ side chain, but it also contacts D187$^{45.51}$ through a water bridge. Moreover, the C-terminal Pen^{7} carboxylate group establishes H-bonds with the Y190$^{45.54}$ phenolic group and the Q200$^{5.39}$ amidic function. Additional contacts are eventually formed by the acetyl cap and the Arg^{1} backbone NH with the N37$^{1.31}$ and E288$^{7.39}$ side chains, respectively. Overall, the binding mode predicted for **19** is in agreement with its subnanomolar potency and with crystallographic and mutagenesis data indicating residues such W94$^{2.60}$, D97$^{2.63}$, H113$^{3.29}$, and Y116$^{3.32}$ in TMS1, H203$^{5.42}$, Y255$^{6.51}$, D262$^{6.58}$, and E288$^{7.39}$ in TMS2, and D187$^{45.51}$ and R188$^{45.52}$ in ECL2 as important for ligand binding to CXCR4.[40] Likewise, previous computational studies revealed that some of the latter residues are crucial for the binding of potent cyclopeptide CXCR4 antagonists. For instance, the potent cyclic pentapeptides developed by Fujii and co-workers, which feature two positively charged (arginine) and two aromatic residues (Tyr and 2-Nal), were predicted to use D97$^{2.63}$ and D187$^{45.51}$ as first anchor points for receptor binding and to

DOI: 10.1021/acs.jmedchem.7b01062
J. Med. Chem. 2017, 60, 9641−9652

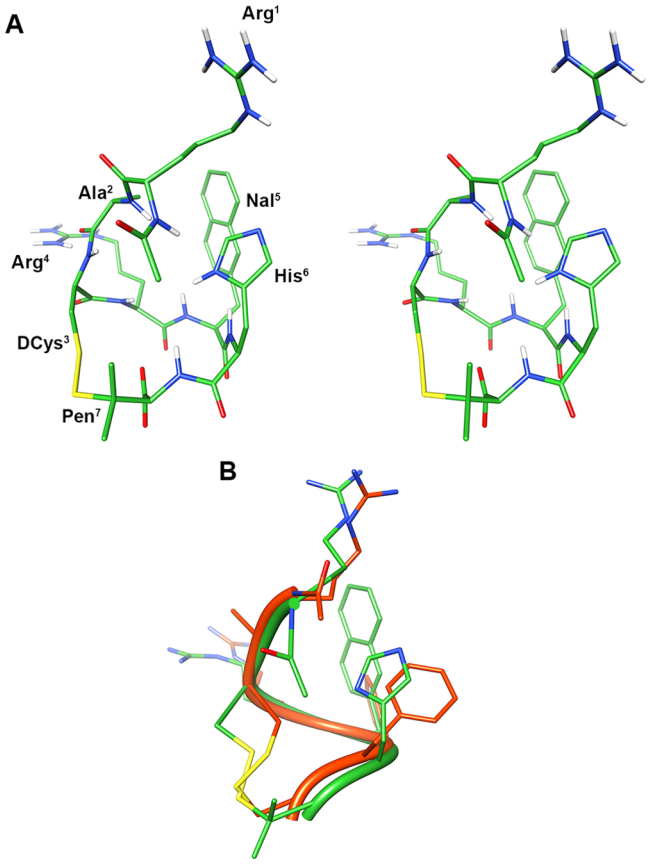

Figure 6. (A) Stereoimage of the lowest energy conformer of **19**. Heavy atoms are represented with different colors (carbon, green; nitrogen, blue; oxygen, red; sulfur, yellow). Nonpolar hydrogen atoms are hidden for clarity reasons. (B) Superposition of the NMR lowest energy conformations of **19** (green) and **3** (orange)[24] on the Cα carbon atoms of residues 3−7.

insert their 2-Nal side chain in the cleft defined by R188$^{45.52}$ and H203$^{5.42}$,[27] similar to **19**. Docking studies would however suggest that the latter ligands use D171$^{4.60}$ as second anchor point,[27] different from our peptide that in fact binds D262$^{6.58}$ and E288$^{7.39}$. On the other hand, a subnanomolar N-alkylated cyclopeptide analogue developed by Demmer et al. was predicted to interact with the side chains of D97$^{2.63}$, D187$^{45.51}$, and D262$^{6.58}$ through its two arginine residues and to form a cation−π with R188$^{45.52}$ through the Nal^4 side chain,[15] in line with the binding mode predicted for **19**. It is also interesting to note that the **19** MD pose is superimposable to that previously described for the lead peptide **3** (Figure 7B),[24] although few differences can be found. Particularly, both the Arg^1 side chain and the C-terminal carboxylate group of **19** directly interact with the target, while in the case of **3** the same moieties are involved in a tight intramolecular interaction. This could be due to the slight different peptide ring arrangement resulting from the L-Cys^7/L-Pen^7 substitution, which in turn might not allow the Arg^1 side chain of **19** to fold toward the C-terminus. Furthermore, the introduction of His (**19**) in place of Phe (**3**) allows the ligand to form additional tight polar contacts, explaining the remarkable increase in the affinity toward CXCR4 (**3**, IC_{50} = 53 nM; **19**, IC_{50} = 1.5 nM). The MD binding pose of **19** also allows us to rationalize the structure−activity relationships of all the other compounds presented in this study. Specifically, (i) as already outlined in our previous study,[24] the nature and the chirality of the amino acids forming the disulfide bond (cysteine and/or penicillamine) are crucial to properly orient the peptide pharmacophoric groups at the CXCR4 receptor; within this framework, the best results have been achieved with peptides featuring D-Cys and L-Pen at the 3 and 7 positions, respectively (compare **4** vs **3**, **5**, and **6**). (ii) At the 5 position, residues featuring side chains bulkier than Phe can establish additional lipophilic or in the aromatic subpocket of the CXCR4 ligand binding site, although they should satisfy specific steric requisites. Actually, the introduction of residues such as (4-Cl)Phe (**9**), 1-Nal (**11**), or 2-Nal (**12**) produces alternative effects on the peptide target affinity; indeed, the latter amino acids are, respectively, well tolerated, unfavorable, or advantageous for the binding to CXCR4. For the same reasons, the presence, at the 5 position, of amino acids bearing more polar side chains (peptides **7**, **8**, and **10**) is always detrimental for the peptide potency. Finally, (iii) at the 6 position, the replacement of Phe with any aromatic residue (peptides **14**−**18**) other than histidine (**13**) always causes a drop in affinity, mainly for steric reasons.

CONCLUSIONS

The overexpression of CXCR4 on the cancer cell membrane, along with the CXCL12 release from secondary organs, cooperates in arranging the environment for metastases nestling.[1−3] Hence, during the past decade various CXCR4 antagonists have been in development as potential antimetastatic agents.[10,12,16,30] In this respect, we have recently reported the plasma stable and selective CXCR4 peptide antagonist Ac-Arg-Ala-[D-Cys-Arg-Phe-Phe-Cys]-COOH (**3**), which however did not yet exhibit the suitable potency (IC_{50} of 53 nM) for in vivo studies. Thus, we here embarked in an extensive lead-optimization campaign of **3**, which led to the identification of a novel potent CXCR4 antagonist (Ac-Arg-Ala-[D-Cys-Arg-2-Nal-His-Pen]-COOH, **19**) endowed with an IC_{50} of 1.5 nM. Remarkably, the binding potency of **19** is comparable to that of plerixafor (**1**), which is the only clinically approved CXCR4 antagonist.[4,30] We also highlight that the chemical modifications applied did affect neither the selectivity nor the stability in biological fluids of **19** which indeed cannot interact with the related CXCR7 and unrelated CXCR3 chemokine receptors and remains unaltered up to 2 h in human serum. Moreover, NMR and advanced molecular modeling studies allowed us to define the structural reasons beyond the improved activity observed for **19** versus the lead peptide **3**. Finally, functional cell-based assays demonstrated that **19** was able to prevent both cell migration and receptor internalization, which are validated hallmarks for CXCR4 antagonism, at low nanomolar concentration and more efficiently than **1**. In light of these data, **19** possesses all the prerequisites, including high affinity, selectivity, and serum stability, that allow this peptide to move toward preclinical investigations aimed to confirm its efficacy in vivo. Likewise, **19** might represent the starting point for the development of novel chemical probes for PET or MRI studies in CXCR4 overexpressing cancers with the final aim to improve and fine-tune CXCR4-targeted therapies, in the modern context of personalized medicine.

EXPERIMENTAL SECTION

Chemistry. Materials. N^{α}-Fmoc-protected amino acids, 2-chlorotrityl chloride (2-Cl-TrtCl) resin, Fmoc-Rink amide-Am resin, *O*-benzotriazole-*N*,*N*,*N*′,*N*′-tetramethyluronium hexafluorophosphate (HBTU), *N*,*N*-diisopropylethylamine (DIPEA), triisopropylsilane

DOI: 10.1021/acs.jmedchem.7b01062
J. Med. Chem. 2017, 60, 9641−9652

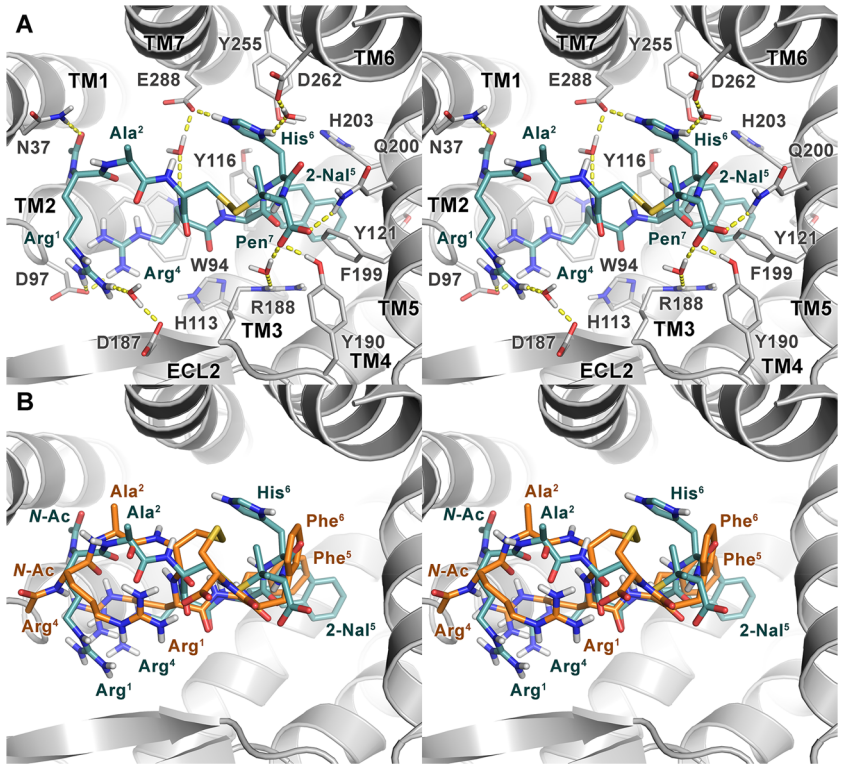

Figure 7. (A) Binding mode of **19** (cyan sticks) at the CXCR4 receptor (gray cartoons) obtained through over 300 ns long MD simulations. Receptor amino acids and waters important for peptide binding are shown as sticks. Hydrogen bonds are displayed as dashed yellow lines. Nonpolar hydrogens are omitted for clarity. (B) Superposition between the MD-predicted binding poses of **3**[24] (orange sticks) and **19** at the CXCR4 receptor (gray cartoons). Both images are shown in stereoview.

(TIS), trifluoroacetic acid (TFA), piperidine, and *N*-hydroxybenzotriazole (HOBt) were from Iris-Biotech Gmbh (Marktredwitz, Germany). *N*,*N*-Dimethylformamide (DMF), dichloromethane (DCM), diethyl ether, *N*-chlorosuccinimide (NCS), H_2O, CH_3CN for HPLC and human serum were reagent grade and were acquired from commercial sources (Sigma-Aldrich, Milano, Italy) and used as received unless otherwise noted. Peptides were purified by preparative HPLC (Shimadzu HPLC system) equipped with a C18-bounded preparative RP-HPLC column (Phenomenex Kinetex 21.2 mm × 150 mm, 5 μm). The purity of all the peptides was ≥95% as confirmed by analytical HPLC (Shimadzu Prominance HPLC system) equipped with a C18-bounded analytical RP-HPLC column (Phenomenex Kinetex, 4.6 mm × 250 mm, 5 μm) using a gradient elution (10−90% acetonitrile in water (0.1% TFA) over 15 min; flow rate = 1.0 mL/min; diode array UV detector). Accurate molecular weights of compounds were confirmed by ESI mass spectrometry using a Q Exactive Orbitrap LC−MS/MS (Thermo Fisher Scientific, Waltham, MA, USA) (Supporting Information Table S1).

General Procedure for the Synthesis of Peptides. 2-Cl-TrtCl resin (93.0 mg, 1.60 mmol/g) was swollen in dry DMF (2 mL) over 0.5 h, and a solution of Fmoc-L-Cys(Trt)-OH (59.0 mg, 0.10 mmol, 0.67 equiv) or Fmoc-L-Pen(Trt)-OH (62.0 mg, 0.10 mmol, 0.67 equiv) and DIPEA (79 μL, 3 equiv) in DMF (2 mL) was added. The mixture was stirred for 24 h. The residual chloride groups contained in the resin were capped by adding MeOH (200 μL) in DCM (2 mL) in the presence of DIPEA (52 μL, 2 equiv) and stirring for 30 min to avoid eventually parallel synthesis of side products. Fmoc group removal was performed using 20% piperidine in DMF (1 × 5 min and 1 × 25 min). The peptide resin was then washed with DCM (3 × 0.5 min) and DMF (3 × 0.5 min), and positive Kaiser ninhydrin[41] and 2,4,6-trinitrobenzenesulfonic acid (TNBS)[42] tests were observed. Fmoc-L-Phe-OH (155.0 mg, 0.4 mmol, 4 equiv) or Fmoc-L-His(Trt)-OH (248.0 mg, 0.4 mmol, 4 equiv) or Fmoc-L-Phg-OH (149.4 mg, 0.4 mmol, 4 equiv) or Fmoc- L-Phe(4-NO_2)-OH (173.0 mg, 0.4 mmol, 4 equiv) or Fmoc-L-Phe(4-Cl)-OH (168.8 mg, 0.4 mmol, 4 equiv) or Fmoc-L-1-Nal-OH (175.0 mg, 0.4 mmol, 4 equiv) or Fmoc-L-2-Nal-OH (175.0 mg, 0.4 mmol, 4 equiv), Fmoc-L-Arg(Pbf)-OH (259. 5 mg, 0.4 mmol, 4 equiv), Fmoc-L-Cys(Trt)-OH (234.3 mg, 0.4 mmol, 4 equiv) or Fmoc-D-Pen(Trt)-OH (245.5 mg, 0.4 mmol, 4 equiv), Fmoc-L-Ala-OH (124.5 mg, 0.4 mmoli, 4 equiv) were sequentially added to the resin bound H-L-Cys(Trt)/L-Pen(Trt). Each coupling reaction was achieved using a 4-fold excess of amino acid with HBTU (151. 7 mg, 0.4 mmol, 4 equiv) and HOBt (61.2 mg, 0.4 mmol, 4 equiv) in the presence of DIPEA (140 μL, 0.8 mmol, 8 equiv) in DMF. Fmoc deprotections were accomplished with 20% piperidine in DMF solution (1 × 5 min, 1 × 25 min). Washings with DMF (3 × 0.5 min) and DCM (3 × 0.5 min) were performed through every coupling/deprotection step. Kaiser ninhydrin and TNBS tests were employed for monitoring the progress of peptide synthesis. After removal of the last Fmoc group, the resin bound peptide was treated with Ac_2O (19 μL, 0.2 mmol, 2 equiv) and DIPEA (70 μL, 0.4 mmol, 2 equiv) in DCM (2 mL) and the mixture was shaken for 1 h. Negative Kaiser ninhydrin and TNBS tests were observed.

General Procedure for Peptide Oxidation and Purification. The peptide was released from the solid support and all the protecting groups were cleaved, treating the resin with TFA/DCM/TIS (80/15/5, v/v/v) (3 mL solvent/0.1 mmol) for 2 h. The resin was then filtered off and the crude linear peptide was recovered by precipitation with chilled ether to give a powder. The crude peptide (0.1 mmol) was dissolved in 45 mL of H_2O, and a solution of NCS (20 mg, 0.15 mmol, 1.5 equiv) in H_2O (5 mL) was added. The mixture was mechanically stirred for 30 min at room temperature.[26] The solution mixture was finally purified by preparative RP-HPLC in 0.1% TFA with an acetonitrile (ACN) gradient (10−70% ACN in H_2O over 20 min, flow rate of 15 mL/min) on a Phenomenex Kinetex C18 column (21.2 mm × 150 mm, 5 μm). Analytical RP-HPLC was performed in 0.1% TFA with an ACN gradient (10−90% ACN in H_2O over 20 min, flow rate of 1.0 mL/min) on a Phenomenex Kinetex C18 column (0.46 mm × 150 mm, 5 μm).

DOI: 10.1021/acs.jmedchem.7b01062
J. Med. Chem. 2017, 60, 9641−9652

CXC Receptors Binding Assays. 5×10^5 CCRF-CEM cells were preincubated with increasing peptide concentrations (ranging from 10 pM to 10 μM) in the binding buffer (PBS 1× plus 0.2% BSA and 0.1% NaN_3) for 30 min at 37 °C, 5% CO_2 and then labeled for 30 min using an anti-CXCR4 PE-antibody (FAB170P, clone 12G5, R&D Systems, Minneapolis, MN, USA). To evaluate the selectivity toward CXCR4 against CXCR3 and CXCR7, the experiments were also performed on the CXCR3-overexpressing COLO205 cell line using a specific anti-CXCR3 antibody (BD Pharmingen 560831 clone 1C6/CXCR3) as well as on the CXCR7-overexpressing MCF-7 cell line using a specific anti-CXCR7 antibody (R&D FAB4227A clone 11G8). A FACSCanto II flow cytometer (B.D. Biosciences, CA, USA) and the Diva version 6.1.1 software were used to collect and analyze the data, respectively.

^{125}I-CXCL12 Competitive Binding. CCRF-CEM cells were harvested and suspended in the binding buffer (PBS containing 5 mM $MgCl_2$, 1 mM $CaCl_2$, 0.25% BSA, pH 7.4) with different ligand (**3** or **19**) concentrations, ranging from 10 pM to 10 μM and in the presence of fixed tracer amounts of the ^{125}I-CXCL12 (PerkinElmer, 2200 Ci/mmol). The amount of bound radioactivity was determined after 1 h at 4 °C using a γ counter and expressed as percent of total counts. IC_{50} values were calculated through the GraphPad Prism software (GraphPad Software Inc., CA).

Migration Assay. Migration was assayed in 24-well Transwell chambers (Corning Inc., Corning, NY) using inserts with 5 and 8 μm (optimal for lymphocytes and epithelial cells, respectively) pore membranes. Membranes were precoated with collagen (human collagen type I/III) and fibronectin (20 μg/mL each). Cells were placed in the upper chamber (2×10^5 cells/well) in culture medium containing 1% BSA (migration media) in the presence of increasing ligand (**1** or **19**) concentrations (from 10 nM to 10 μM); 100 ng/mL CXCL12 was added to the lower chamber. After 18 h incubation, cells atop the filter were removed using a cotton wool swab; migration of cells in the alone medium (control) was compared with that observed in media containing CXCL12. The cells were counted in 10 different fields (original 400× magnification). The migration index was defined as the ratio between migrating cells in the experimental group and migrated cells in the control group.

CXCR4 Internalization Assay. To create the CHO-CXCR4-GFP cell line, the pEGFP-CXCR4 plasmid was transfected by TurboFectin 8.0 (OriGene) in accordance with the manufacturer's instructions. CHO-CXCR4-GFP cells were grown on 10 mm coverslips in DMEM containing 10% FBS for 1 day, washed with PBS−0.5% BSA, and equilibrated in DMEM−0.5% BSA. Cells were preincubated with **1** or **19** at 10 nM for 45 min at 37 °C. Then, they were then treated with CXCL12 (12.5 nM) and incubated at 37 °C for different time intervals (30 min, 2 h, 6 h, and 24 h), fixed with 4% formaldehyde for 10 min, washed three times in PBS, and inspected with a Zeiss LSM 510 confocal microscope.

Serum Biostability Assay. Serum stability was evaluated applying a previously described protocol.[32] Briefly, the reaction solution was prepared by mixing 10 μL of water solution of peptide (1 mM) and 90 μL of human serum (at concentration 0.1 mM, 90% serum) and incubated at 37 °C. Aliquots were collected at different times (0, 15 min, 30 min, 60 min, 90 min, and 120 min), subjected to precipitation by addition of ACN (0.1% TFA) solution, and then centrifuged (12 000 rpm, 15 min, 4 °C). The supernatant obtained was analyzed by HPLC using a linear elution gradient from 10% to 90% ACN (0.1% TFA) in water (0.1% TFA) in 30 min.

NMR Spectroscopy. The samples for NMR spectroscopy were prepared by dissolving the appropriate amount of **19** in 540 μL of ^1H_2O (pH 5.5), 60 μL of ^2H_2O to obtain a concentration 2 mM of peptide and 200 mM of SDS-d_{25}. NMR spectra were recorded on a Varian INOVA 700 MHz spectrometer equipped with a z-gradient 5 mm triple-resonance probe head in a 5 mm tube. The spectra were calibrated relative to TSP (0.00 ppm) as internal standard. 1D and 2D NMR spectra were recorded and processed as previously described.[24] $^3J_{HN\text{-}H\alpha}$ coupling constants were obtained from 1D ^{1}H NMR and 2D DQF-COSY spectra. The temperature coefficients of the amide proton chemical shifts were calculated from 1D ^{1}H NMR and 2D TOCSY experiments performed at different temperatures in the range 25−35 °C by means of linear regression. The NOE-based distance restraints were obtained from NOESY spectra collected with a 100 ms mixing time. The NOE cross peaks were integrated with the XEASY program[37] and were converted into upper distance bounds using the CALIBA program incorporated into the DYANA program package.[43] An error-tolerant target function (tf-type = 3) was used to account for the peptide intrinsic flexibility. From the produced 100 conformations, 10 structures were chosen, whose interproton distances best fitted NOE derived distances, and then refined through successive steps of restrained and unrestrained energy minimization using the Discover algorithm (Accelrys, San Diego, CA) and the consistent valence force field (CVFF).[44] Molecular graphics images of the ensemble and the overlapped structures of **3** and **19** were produced using the UCSF Chimera package.[45]

Molecular Modeling. A manual docking of the **19** lowest energy conformation in the crystal structure of CXCR4 (PDB code 3OE0)[46] was first accomplished according to the procedure described in our previous publication.[24] The obtained complex was then prepared for submission to MD calculations. In detail, the receptor structure was refined using the protocol described in the same paper.[24] For the ligand, every possible protomeric and tautomeric state of the His^6 residue was taken into account; therefore, three distinct **19**/CXCR4 complexes were set up. Each complex was then embedded in a 1-palmitoyl-2-oleoylphosphatidylcholine (POPC) phospholipids bilayer mimicking the membrane environment. Specifically, a 94 Å × 94 Å (along the x and y axes) pre-equilibrated POPC phospholipid bilayer was first created through the membrane-builder tool of CHARMM-GUI.org (http://www.charmm-gui.org). Then, a hole was generated into the bilayer to host the complex, and all lipids in close contact with the receptor (<1 Å distant from any protein atoms) were deleted. Each complex was then solvated according to the TIP3 water model[47] through the solvation module of VMD 1.9.3. Cl^- counterions were added to each system to ensure neutrality. The ff14SB[48] and lipid14[49] Amber force fields were used to parametrize the protein and the peptide, and the lipids, respectively. Missing parameters for the peptide 2-Nal^5 and Pen^7 residues were generated with Antechamber.[50] Specifically, charges were computed using the restrained electrostatic potential (RESP) fitting procedure.[51] The ESP was first calculated by means of the Gaussian 09 package[52] using a 6-31G* basis set at the Hartree−Fock level of theory, and then the RESP charges were obtained by a two-stage fitting procedure using Antechamber.[50] Missing bonds, angles, torsion and improper torsion angle parameters were then generated using the same program. Each complex was then submitted to over 200 ns MD simulations with NAMD 2.10.[53] A 10 Å cutoff (switched at 8 Å) was used to calculate atom−pair interactions. The long-range electrostatic interactions were computed by means of the particle mesh Ewald (PME) method using a 1.0 Å grid spacing in periodic boundary conditions. The RATTLE algorithm was applied to constrain bonds involving hydrogen atoms, thus allowing the use of a 2 fs integration time step interval. Each system was minimized and heated up to 300 K while applying harmonic constraints, which were gradually released along the equilibration process. To prevent any distortion in the receptor transmembrane helices, their Cα carbons were constrained for further 10 ns. Production run was then performed in the *NPT* ensemble at 1 atm and 300 K. At the end of MD calculations, all the trajectories were carefully inspected to evaluate their rate of agreement with the experimental data. The best results were observed for the complex with the ligand His^6 in the protonated form, which was thus selected for further analysis.

CXCR4 residues were numbered according to both the wild-type primary sequence and the Ballesteros−Weinstein scheme[54] (as superscript).

All of the pictures were rendered using PyMOL (www.pymol.org).

■ ASSOCIATED CONTENT

Supporting Information

The Supporting Information is available free of charge on the ACS Publications website at DOI: 10.1021/acs.jmedchem.7b01062.

DOI: 10.1021/acs.jmedchem.7b01062
J. Med. Chem. 2017, 60, 9641−9652

Analytical data for the studied peptides; NMR resonance assignments of **19**; NOE derived upper limit constraints of **19**; Cα carbons rmsd of **19** along the MD production run (PDF)

Model of **19** at the CXCR4 binding site (PDB)

Accession Codes

The PDB code is 5OJT for the NMR structure of **19**. Authors will release the atomic coordinates and experimental data upon article publication.

AUTHOR INFORMATION

Corresponding Authors

*S.S.: phone, 0039-081-5903678, 0039-380-3140318; e-mail, s.scala@istitutotumori.na.it.

*L.M.: phone, 0039-328-6795645; e-mail, lmarinel@unina.it.

ORCID

Ettore Novellino: 0000-0002-2181-2142

Luciana Marinelli: 0000-0002-4084-8044

Author Contributions

$^{\perp}$S.D.M., F.S.D.L., and A.M.T. equally contributed to this work. The manuscript was written through contributions from all authors. All authors have given approval to the final version of the manuscript.

Notes

The authors declare no competing financial interest.

ACKNOWLEDGMENTS

This research was funded by Scientific Independence of Young Researchers (SIR) 2014 (Grant RBSI142AMA) to S.D.M, MIUR-PRIN 2015 (Grant FCHJ8E) to L.M., and Euro-Nanomed (Nano) systems with active targeting to sensitize colorectal cancer stem cells to antitumoral treatment (Target4Cancer) to S.S.

ABBREVIATIONS USED

ACN, acetonitrile; APC, allophycocyanin; CAF, cancer-associated fibroblast; CCL, CC chemokine ligand; CCR, CC chemokine receptor; CXCL, CC chemokine ligand; CXCR, CXC chemokine receptor; CVFF, consistent valence force field; DIPEA, *N*,*N*-diisopropylethylamine; DMEM, Dulbecco's modified Eagle's medium; DQF, double quantum filter; ECL, extracellular loop; ESP, electrostatic potential; FBS, fetal bovine serum; FITC, fluorescein isothiocyanate; GPCR, G-protein-coupled receptor; GSK3, glycogen synthase kinase 3; HBTU, *O*-benzotriazole-*N*,*N*,*N*′,*N*′-tetramethyluronium hexafluorophosphate; HOBt, *N*-hydroxybenzotriazole; IC, inhibitory concentration; ICR, immune checkpoint receptor; MMP2, matrix metalloproteinase 2; mTOR, mammalian target of rapamycin; Nal, naphthylalanine; PE, phycoerythrin; POPC, 1-palmitoyl-2-oleoylphosphatidylcholine; SAR, structure−activity relationship; RESP, restrained electrostatic potential; SD, standard deviation; SDF-1α, stromal cell derived factor 1α; SDS, sodium dodecyl sulfate; STAT3, signal transducer and activator of transcription 3; TIS, triisopropylsilane; TIMP-1, TIMP metallopeptidase inhibitor 1; TNBS, 2,4,6-trinitrobenzenesulfonic acid; TOCSY, total correlation spectroscopy; VEGF, vascular endothelial growth factor

REFERENCES

(1) (a) Kochetkova, M.; Kumar, S.; McColl, S. R. Chemokine receptors CXCR4 and CCR7 promote metastasis by preventing anoikis in cancer cells. *Cell Death Differ.* **2009**, *16*, 664−673. (b) Mukherjee, D.; Zhao, J. The role of chemokine receptor CXCR4 in breast cancer metastasis. *Am. J. Cancer Res.* **2013**, *3*, 46−57.

(2) Chatterjee, S.; Azad, B. B.; Nimmagadda, S. The intricate role of CXCR4 in cancer. *Adv. Cancer Res.* **2014**, *124*, 31−82.

(3) Peinado, H. C. A.; Zhang, H.; Matei, I. R.; Costa-Silva, B.; Hoshino, A.; Rodrigues, G.; Psaila, B.; Kaplan, R. N.; Bromberg, J. F.; Kang, Y.; Bissell, M. J.; Cox, T. R.; Giaccia, A. J.; Erler, J. T.; Hiratsuka, S.; Ghajar, C. M.; Lyden, D. Pre-metastatic niches: organ-specific homes for metastases. *Nat. Rev. Cancer* **2017**, *17*, 302−317.

(4) (a) De Clercq, E.; Yamamoto, N.; Pauwels, R.; Balzarini, J.; Witvrouw, M.; De Vreese, K.; Debyser, Z.; Rosenwirth, B.; Peichl, P.; Datema, R. Highly potent and selective inhibition of human immunodeficiency virus by the bicyclam derivative JM3100. *Antimicrob. Agents Chemother.* **1994**, *38*, 668−674. (b) Donzella, G. A.; Schols, D.; Lin, S. W.; Este, J. A.; Nagashima, K. A.; Maddon, P. J.; Allaway, G. P.; Sakmar, T. P.; Henson, G.; De Clercq, E.; Moore, J. P. AMD3100, a small molecule inhibitor of HIV-1 entry via the CXCR4 co-receptor. *Nat. Med.* **1998**, *4*, 72−77. (c) De Clercq, E. The bicyclam AMD3100 story. *Nat. Rev. Drug Discovery* **2003**, *2*, 581−587.

(5) Seubert, B.; Grünwald, B.; Kobuch, J.; Cui, H.; Schelter, F.; Schaten, S.; Siveke, J. T.; Lim, N. H.; Nagase, H.; Simonavicius, N.; Heikenwalder, M.; Reinheckel, T.; Sleeman, J. P.; Janssen, K.-P.; Knolle, P. A.; Krüger, A. Tissue inhibitor of metalloproteinases (TIMP)-1 creates a premetastatic niche in the liver through SDF-1/CXCR4-dependent neutrophil recruitment in mice. *Hepatology* **2015**, *61*, 238−248.

(6) (a) Ling, X.; Spaeth, E.; Chen, Y.; Shi, Y.; Zhang, W.; Schober, W.; Hail, N.; Konopleva, M.; Andreeff, M. The CXCR4 antagonist AMD3465 regulates oncogenic signaling and invasiveness in Vitro and prevents breast cancer growth and metastasis in vivo. *PLoS One* **2013**, *8*, e58426. (b) Guo, F.; Wang, Y.; Liu, J.; Mok, S. C.; Xue, F.; Zhang, W. CXCL12/CXCR4: a symbiotic bridge linking cancer cells and their stromal neighbors in oncogenic communication networks. *Oncogene* **2016**, *35*, 816−826.

(7) (a) Scala, S. Molecular pathways: targeting the CXCR4-CXCL12 axis−untapped potential in the tumor microenvironment. *Clin. Cancer Res.* **2015**, *21*, 4278−4285. (b) Mahoney, M. K.; Rennert, D. P.; Freeman, G. J. Combination cancer immunotherapy and new immunomodulatory targets. *Nat. Rev. Drug Discovery* **2015**, *14*, 561−84.

(8) Xing, Y.; Zhao, S.; Zhou, B. P.; Mi, J. Metabolic reprogramming of the tumour microenvironment. *FEBS J.* **2015**, *282*, 3892−3898.

(9) Braun, M.; Qorraj, M.; Büttner, M.; Klein, F. A.; Saul, D.; Aigner, M.; Huber, W.; Mackensen, A.; Jitschin, R.; Mougiakakos, D. CXCL12 promotes glycolytic reprogramming in acute myeloid leukemia cells via the CXCR4/mTOR axis. *Leukemia* **2016**, *30*, 1788−1792.

(10) (a) Karpova, D.; Dauber, K.; Spohn, G.; Chudziak, D.; Wiercinska, E.; Schulz, M.; Pettit, A. R.; Levesque, J. P.; Romagnoli, B.; Patel, K.; Chevalier, E.; Dembowsky, K.; Bonig, H. The novel CXCR4 antagonist POL5551 mobilizes hematopoietic stem and progenitor cells with greater efficiency than plerixafor. *Leukemia* **2013**, *27*, 2322−2331. (b) Sison, E. A. R.; Magoon, D.; Li, L.; Annesley, C. E.; Romagnoli, B.; Douglas, G. J.; Tuffin, G.; Zimmermann, J.; Brown, P. POL5551, a novel and potent CXCR4 antagonist, enhances sensitivity to chemotherapy in pediatric ALL. *Oncotarget* **2015**, *6*, 30902−30918.

(11) Tamamura, H.; Xu, Y.; Hattori, T.; Zhang, X.; Arakaki, R.; Kanbara, K.; Omagari, A.; Otaka, A.; Ibuka, T.; Yamamoto, N.; Nakashima, H.; Fujii, N. A low-molecular-weight inhibitor against the chemokine receptor CXCR4: a strong anti-HIV peptide T140. *Biochem. Biophys. Res. Commun.* **1998**, *253*, 877−882.

(12) Tamamura, H.; Hori, A.; Kanzaki, N.; Hiramatsu, K.; Mizumoto, M.; Nakashima, H.; Yamamoto, N.; Otaka, A.; Fujii, N. T140 analogs as CXCR4 antagonists identified as anti-metastatic agents in the treatment of breast cancer. *FEBS Lett.* **2003**, *550*, 79−83.

(13) Kobayashi, K.; Oishi, S.; Hayashi, R.; Tomita, K.; Kubo, T.; Tanahara, N.; Ohno, H.; Yoshikawa, Y.; Furuya, T.; Hoshino, M.; Fujii, N. Structure-activity relationship study of a CXC chemokine

DOI: 10.1021/acs.jmedchem.7b01062
J. Med. Chem. 2017, 60, 9641−9652

receptor type 4 antagonist, FC131, using a series of alkene dipeptide isosteres. *J. Med. Chem.* **2012**, *55*, 2746−2757.
(14) Mungalpara, J.; Thiele, S.; Eriksen, Ø.; Eksteen, J.; Rosenkilde, M. M.; Våbenø, J. Rational design of conformationally constrained cyclopentapeptide antagonists for C-X-C chemokine receptor 4 (CXCR4). *J. Med. Chem.* **2012**, *55*, 10287−10291.
(15) (a) Demmer, O.; Dijkgraaf, I.; Schumacher, U.; Marinelli, L.; Cosconati, S.; Gourni, E.; Wester, H. J.; Kessler, H. Design, synthesis, and functionalization of dimeric peptides targeting chemokine receptor CXCR4. *J. Med. Chem.* **2011**, *54*, 7648−7662. (b) Demmer, O.; Frank, A. O.; Hagn, F.; Schottelius, M.; Marinelli, L.; Cosconati, S.; Brack-Werner, R.; Kremb, S.; Wester, H. J.; Kessler, H. A conformationally frozen peptoid boosts CXCR4 affinity and anti-HIV activity. *Angew. Chem., Int. Ed.* **2012**, *51*, 8110−8113.
(16) (a) Peng, S. B.; Zhang, X.; Paul, D.; Kays, L. M.; Gough, W.; Stewart, J.; Uhlik, M. T.; Chen, Q.; Hui, Y. H.; Zamek-Gliszczynski, M. J.; Wijsman, J. A.; Credille, K. M.; Yan, L. Z. Identification of LY2510924, a novel cyclic peptide CXCR4 antagonist that exhibits antitumor activities in solid tumor and breast cancer metastatic models. *Mol. Cancer Ther.* **2015**, *14*, 480−490. (b) Hainsworth, J. D.; Reeves, J. A.; Mace, J. R.; Crane, E. J.; Hamid, O.; Stille, J. R.; Flynt, A.; Roberson, S.; Polzer, J.; Arrowsmith, E. R. A Randomized, open-label phase 2 study of the CXCR4 inhibitor LY2510924 in combination with sunitinib versus sunitinib alone in patients with metastatic renal cell carcinoma (RCC). *Target Oncol.* **2016**, *11*, 643−653. (c) Salgia, R.; Stille, J. R.; Weaver, R. W.; McCleod, M.; Hamid, O.; Polzer, J.; Roberson, S.; Flynt, A.; Spigel, D. R. A randomized phase II study of LY2510924 and carboplatin/etoposide versus carboplatin/etoposide in extensive-disease small cell lung cancer. *Lung Cancer* **2017**, *105*, 7−13.
(17) (a) Ros-Blanco, L.; Anido, J.; Bosser, R.; Esté, J.; Clotet, B.; Kosoy, A.; Ruíz-Ávila, L.; Teixidó, J.; Seoane, J.; Borrell, J. I. Noncyclam tetraamines inhibit CXC chemokine receptor type 4 and target glioma-initiating cells. *J. Med. Chem.* **2012**, *55*, 7560−7570. (b) Truax, V. M.; Zhao, H.; Katzman, B. M.; Prosser, A. R.; Alcaraz, A. A.; Saindane, M. T.; Howard, R. B.; Culver, D.; Arrendale, R. F.; Gruddanti, P. R.; Evers, T. J.; Natchus, M. G.; Snyder, J. P.; Liotta, D. C.; Wilson, J. L. Discovery of tetrahydroisoquinoline-based CXCR4 antagonists. *ACS Med. Chem. Lett.* **2013**, *4*, 1025−1030. (c) Zachariassen, Z. G.; Karlshøj, S.; Haug, B. E.; Rosenkilde, M. M.; Våbenø, J. Probing the molecular interactions between CXC chemokine receptor 4 (CXCR4) and an arginine-based tripeptidomimetic antagonist (KRH-1636). *J. Med. Chem.* **2015**, *58*, 8141−8153.
(18) (a) Demmer, O.; Gourni, E.; Schumacher, U.; Kessler, H.; Wester, H. J. PET imaging of CXCR4 receptors in cancer by a new optimized ligand. *ChemMedChem* **2011**, *6*, 1789−1791. (b) Philipp-Abbrederis, K.; Herrmann, K.; Knop, S.; Schottelius, M.; Eiber, M.; Luckerath, K.; Pietschmann, E.; Habringer, S.; Gerngross, C.; Franke, K.; Rudelius, M.; Schirbel, A.; Lapa, C.; Schwamborn, K.; Steidle, S.; Hartmann, E.; Rosenwald, A.; Kropf, S.; Beer, A. J.; Peschel, C.; Einsele, H.; Buck, A. K.; Schwaiger, M.; Götze, K.; Wester, H. J.; Keller, U. In vivo molecular imaging of chemokine receptor CXCR4 expression in patients with advanced multiple myeloma. *EMBO Mol. Med.* **2015**, *7*, 477−487. (c) Lesniak, W. G.; Sikorska, E.; Shallal, H.; Azad, B. B.; Lisok, A.; Pullambhatla, M.; Pomper, M. G.; Nimmagadda, S. Structural characterization and in vivo evaluation of β-hairpin peptidomimetics as specific CXCR4 imaging agents. *Mol. Pharmaceutics* **2015**, *12*, 941−953. (d) Zhao, Y.; Detering, L.; Sultan, D.; Cooper, M. L.; You, M.; Cho, S.; Meier, S. L.; Luehmann, H.; Sun, G.; Rettig, M.; Dehdashti, F.; Wooley, K. L.; DiPersio, J. F.; Liu, Y. Gold nanoclusters doped with ^{64}Cu for CXCR4 positron emission tomography imaging of breast cancer and metastasis. *ACS Nano* **2016**, *10*, 5959−5970. (e) Vag, T.; Gerngross, C.; Herhaus, P.; Eiber, M.; Philipp-Abbrederis, K.; Graner, F. P.; Ettl, J.; Keller, U.; Wester, H. J.; Schwaiger, M. First experience with chemokine receptor CXCR4-targeted PET imaging of patients with solid cancers. *J. Nucl. Med.* **2016**, *57*, 741−746.
(19) (a) Weiss, I. D.; Jacobson, O.; Kiesewetter, D. O.; Jacobus, J. P.; Szajek, L. P.; Chen, X.; Farber, J. M. Positron emission tomography imaging of tumors expressing the human chemokine receptor CXCR4 in mice with the use of ^{64}Cu-AMD3100. *Mol. Imaging Biol.* **2012**, *14*, 106−114. (b) Woodard, L. E.; De Silva, R. A.; Behnam Azad, B.; Lisok, A.; Pullambhatla, M.; Lesniak, W. G.; Mease, R. C.; Pomper, M. G.; Nimmagadda, S. Bridged cyclams as imaging agents for chemokine receptor 4 (CXCR4). *Nucl. Med. Biol.* **2014**, *41*, 552−561.
(20) Oltmanns, D.; Zitzmann-Kolbe, S.; Mueller, A.; Bauder-Wuest, U.; Schaefer, M.; Eder, M.; Haberkorn, U.; Eisenhut, M. Zn(II)-bis(cyclen) complexes and the imaging of apoptosis/necrosis. *Bioconjugate Chem.* **2011**, *22*, 2611−2624.
(21) Hartimath, S. V.; van Waarde, A.; Dierckx, R. A. J. O.; de Vries, E. F. J. Evaluation of *N*-[^{11}C]methyl-AMD3465 as a PET tracer for imaging of CXCR4 receptor expression in a C6 glioma tumor model. *Mol. Pharmaceutics* **2014**, *11*, 3810−3817.
(22) (a) Wester, H. J.; Keller, U.; Schottelius, M.; Beer, A.; Philipp-Abbrederis, K.; Hoffmann, F.; Simecek, J.; Gerngross, C.; Lassmann, M.; Herrmann, K.; Pellegata, N.; Rudelius, M.; Kessler, H.; Schwaiger, M. Disclosing the CXCR4 expression in lymphoproliferative diseases by targeted molecular imaging. *Theranostics* **2015**, *5*, 618−630. (b) Lapa, C.; Lückerath, K.; Rudelius, M.; Schmid, J. S.; Schoene, A.; Schirbel, A.; Samnick, S.; Pelzer, T.; Buck, A. K.; Kropf, S.; Wester, H. J.; Herrmann, K. [^{68}Ga]pentixafor-PET/CT for imaging of chemokine receptor 4 expression in small cell lung cancer-initial experience. *Oncotarget* **2016**, *7*, 9288−9295. (c) Lapa, C.; Lückerath, K.; Kleinlein, I.; Monoranu, C. M.; Linsenmann, T.; Kessler, A. F.; Rudelius, M.; Kropf, S.; Buck, A. K.; Ernestus, R. I.; Wester, H. J.; Löhr, M.; Herrmann, K. ^{68}Ga-pentixafor-PET/CT for imaging of chemokine receptor 4 expression in glioblastoma. *Theranostics* **2016**, *6*, 428−434. (d) Poschenrieder, A.; Schottelius, M.; Schwaiger, M.; Wester, H. J. Preclinical evaluation of [^{68}Ga]NOTA-pentixafor for PET imaging of CXCR4 expression in vivo—a comparison to [^{68}Ga]pentixafor. *EJNMMI Res.* **2016**, *6*, 70.
(23) Portella, L.; Vitale, R.; De Luca, S.; D'Alterio, C.; Ierano, C.; Napolitano, N.; Riccio, A.; Polimeno, M. N.; Monfregola, L.; Barbieri, A.; Luciano, A.; Ciarmiello, A.; Arra, C.; Castello, G.; Amodeo, P.; Scala, S. Preclinical development of a novel class of CXCR4 antagonist impairing solid tumors growth and metastases. *PLoS One* **2013**, *8*, e74548.
(24) Di Maro, S.; Trotta, A. M.; Brancaccio, D.; Di Leva, F. S.; La Pietra, V.; Ieranò, C.; Napolitano, M.; Portella, L.; D'Alterio, C.; Siciliano, R. A.; Sementa, D.; Tomassi, S.; Carotenuto, A.; Novellino, E.; Scala, S.; Marinelli, L. Exploring the N-terminal region of C-X-C motif chemokine 12 (CXCL12): Identification of plasma-stable cyclic peptides as novel, potent C-X-C chemokine receptor type 4 (CXCR4) antagonists. *J. Med. Chem.* **2016**, *59*, 8369−8380.
(25) Barlos, K.; Chatzi, O.; Gatos, D.; Stavropoulos, G. 2-Chlorotrityl chloride resin. Studies on anchoring of Fmoc-amino acids and peptide cleavage. *Int. J. Pept. Protein Res.* **1991**, *37*, 513−520.
(26) (a) Postma, T. M.; Albericio, F. *N*-Chlorosuccinimide, an efficient peptide disulfide bond-forming reagent in aqueous solution. *RSC Adv.* **2013**, *3*, 14277−14280. (b) Postma, T. M.; Albericio, F. *N*-Chlorosuccinimide, an efficient reagent for on-resin disulfide formation in solid-phase peptide synthesis. *Org. Lett.* **2013**, *15*, 616−619.
(27) Thiele, S.; Mungalpara, J.; Steen, A.; Rosenkilde, M. M.; Våbenø, J. Determination of the binding mode for the cyclopentapeptide CXCR4 antagonist FC131 using a dual approach of ligand modifications and receptor mutagenesis. *Br. J. Pharmacol.* **2014**, *171*, 5313−5329.
(28) Grieco, P.; Carotenuto, A.; Campiglia, P.; Zampelli, E.; Patacchini, R.; Maggi, C. A.; Novellino, E.; Rovero, P. A new, potent urotensin II receptor peptide agonist containing a Pen residue at the disulphide bridge. *J. Med. Chem.* **2002**, *45*, 4391−4394.
(29) Fricker, S. P.; Anastassov, V.; Cox, J.; Darkes, M. C.; Grujic, O.; Idzan, S. R.; Labrecque, J.; Lau, G.; Mosi, R. M.; Nelson, K. L.; Qin, L.; Santucci, Z.; Wong, R. S. Y. Characterization of the molecular pharmacology of AMD3100: a specific antagonist of the G-protein coupled chemokine receptor, CXCR4. *Biochem. Pharmacol.* **2006**, *72*, 588−596.

DOI: 10.1021/acs.jmedchem.7b01062
J. Med. Chem. 2017, 60, 9641−9652

(30) DiPersio, J. F.; Micallef, I. N.; Stiff, P. J.; Bolwell, B. J.; Maziarz, R. T.; Jacobsen, E.; Nademanee, A.; McCarty, J.; Bridger, G.; Calandra, G. Phase III prospective randomized double-blind placebo-controlled trial of plerixafor plus granulocyte colony-stimulating factor compared with placebo plus granulocyte colony-stimulating factor for autologous stem-cell mobilization and transplantation for patients with non-Hodgkin's lymphoma. *J. Clin. Oncol.* **2009**, *27*, 4767−4773.
(31) Haribabu, B.; Richardson, R. M.; Fisher, I.; Sozzani, S.; Peiper, S. C.; Horuk, R.; Ali, H.; Snyderman, R. Regulation of human chemokine receptors CXCR4. Role of phosphorylation in desensitization and internalization. *J. Biol. Chem.* **1997**, *272*, 28726−28731.
(32) Mercurio, M. E.; Tomassi, S.; Gaglione, M.; Russo, R.; Chambery, A.; Lama, S.; Stiuso, P.; Cosconati, S.; Novellino, E.; Di Maro, S.; Messere, A. Switchable protecting strategy for solid phase synthesis of DNA and RNA interacting nucleopeptides. *J. Org. Chem.* **2016**, *81*, 11612−11625.
(33) Wüthrich, K. *NMR of Proteins and Nucleic Acids*; John Wiley & Sons, Inc.: New York, 1986.
(34) (a) Piantini, U.; Sorensen, O. W.; Ernst, R. R. Multiple quantum filters for elucidating NMR coupling network. *J. Am. Chem. Soc.* **1982**, *104*, 6800−6801. (b) Marion, D.; Wüthrich, K. Application of phase sensitive two-dimensional correlated spectroscopy (COSY) for measurements of ^{1}H-^{1}H spin-spin coupling constants in proteins. *Biochem. Biophys. Res. Commun.* **1983**, *113*, 967−974.
(35) Braunschweiler, L.; Ernst, R. R. Coherence transfer by isotropic mixing: application to proton correlation spectroscopy. *J. Magn. Reson.* **1983**, *53*, 521−528.
(36) Jeener, J.; Meier, B. H.; Bachmann, P.; Ernst, R. R. Investigation of exchange processes by two-dimensional NMR spectroscopy. *J. Chem. Phys.* **1979**, *71*, 4546−4553.
(37) Bartels, C.; Xia, T.; Billeter, M.; Guentert, P.; Wüthrich, K. The program XEASY for computer-supported NMR spectral analysis of biological macromolecules. *J. Biomol. NMR* **1995**, *6*, 1−10.
(38) Sargent, D. F.; Schwyzer, R. Membrane lipid phase as catalyst for peptide-receptor interactions. *Proc. Natl. Acad. Sci. U. S. A.* **1986**, *83*, 5774−5778.
(39) (a) Grieco, P.; Brancaccio, D.; Novellino, E.; Hruby, V. J.; Carotenuto, A. Conformational study on cyclic melanocortin ligands and new insight into their binding mode at the MC4 receptor. *Eur. J. Med. Chem.* **2011**, *46*, 3721−3733. (b) Mollica, A.; Carotenuto, A.; Novellino, E.; Limatola, A.; Costante, R.; Pinnen, F.; Stefanucci, A.; Pieretti, S.; Borsodi, A.; Samavati, R.; Zador, F.; Benyhe, S.; Davis, P.; Porreca, F.; Hruby, V. J. Novel cyclic biphalin analogue with improved antinociceptive properties. *ACS Med. Chem. Lett.* **2014**, *5*, 1032−1036.
(40) Arimont, M.; Sun, S. L.; Leurs, R.; Smit, M.; de Esch, I. J. P.; de Graaf, C. Structural analysis of chemokine receptor−ligand interactions. *J. Med. Chem.* **2017**, *60*, 4735−4779.
(41) Kaiser, E.; Colescott, R. L.; Bossinger, C. D.; Cook, P. I. Color test for detection of free terminal amino groups in the solid-phase synthesis of peptides. *Anal. Biochem.* **1970**, *34*, 595−598.
(42) Hancock, W. S.; Battersby, J. E. A new micro-test for the detection of incomplete coupling reactions in solid-phase peptide synthesis using 2,4,6-trinitrobenzenesulphonic acid. *Anal. Biochem.* **1976**, *71*, 260−264.
(43) Güntert, P.; Mumenthaler, C.; Wüthrich, K. Torsion angle dynamics for NMR structure calculation with the new program DYANA. *J. Mol. Biol.* **1997**, *273*, 283−298.
(44) Maple, J.; Dinur, U.; Hagler, A. T. Derivation of force fields for molecular mechanics and dynamics from ab initio energy surface. *Proc. Natl. Acad. Sci. U. S. A.* **1988**, *85*, 5350−5353.
(45) Pettersen, E. F.; Goddard, T. D.; Huang, C. C.; Couch, G. S.; Greenblatt, D. M.; Meng, E. C.; Ferrin, T. E. UCSF Chimera - A visualization system for exploratory research and analysis. *J. Comput. Chem.* **2004**, *25*, 1605−1612.
(46) Wu, B.; Chien, E. Y. T.; Mol, C. D.; Fenalti, G.; Liu, W.; Katritch, V.; Abagyan, R.; Brooun, A.; Wells, P.; Bi, F. C.; Hamel, D. J.; Kuhn, P.; Handel, T. M.; Cherezov, V.; Stevens, R. C. Structures of the CXCR4 chemokine receptor in complex with small molecule and cyclic peptide antagonists. *Science* **2010**, *330*, 1066−1071.
(47) Jorgensen, W. L.; Maxwell, D. S.; Tirado-Rives, J. Development and testing of the OPLS all-atom force field on conformational energetics and properties of organic liquids. *J. Am. Chem. Soc.* **1996**, *118*, 11225−11236.
(48) Maier, J. A.; Martinez, C.; Kasavajhala, K.; Wickstrom, L.; Hauser, K. E.; Simmerling, C. ff14SB: improving the accuracy of protein side chain and backbone parameters from ff99SB. *J. Chem. Theory Comput.* **2015**, *11*, 3696−3713.
(49) Dickson, C. J.; Madej, B. D.; Skjevik, A. A.; Betz, R. M.; Teigen, K.; Gould, I. R.; Walker, R. C. Lipid14: the amber lipid force field. *J. Chem. Theory Comput.* **2014**, *10*, 865−879.
(50) Wang, J.; Wang, W.; Kollman, P. A.; Case, D. A. Automatic atom type and bond type perception in molecular mechanical calculations. *J. Mol. Graphics Modell.* **2006**, *25*, 247−260.
(51) Bayly, C. I.; Cieplak, P.; Cornell, W.; Kollman, P. A. A well-behaved electrostatic potential based method using charge restraints for deriving atomic charges: the RESP model. *J. Phys. Chem.* **1993**, *97*, 10269−10280.
(52) Frisch, M. J.; Trucks, G. W.; Schlegel, H. B.; Scuseria, G. E.; Robb, M. A.; Cheeseman, J. R.; Scalmani, G.; Barone, V.; Mennucci, B.; Petersson, G. A.; Nakatsuji, H.; Caricato, M.; Li, X.; Hratchian, H. P.; Izmaylov, A. F.; Bloino, J.; Zheng, G.; Sonnenberg, J. L.; Hada, M.; Ehara, M.; Toyota, K.; Fukuda, R.; Hasegawa, J.; Ishida, M.; Nakajima, T.; Honda, Y.; Kitao, O.; Nakai, H.; Vreven, T.; Montgomery, J. A., Jr.; Peralta, J. E.; Ogliaro, F.; Bearpark, M.; Heyd, J. J.; Brothers, E.; Kudin, K. N.; Staroverov, V. N.; Kobayashi, R.; Normand, J.; Raghavachari, K.; Rendell, A.; Burant, J. C.; Iyengar, S. S.; Tomasi, J.; Cossi, M.; Rega, N.; Millam, N. J.; Klene, M.; Knox, J. E.; Cross, J. B.; Bakken, V.; Adamo, C.; Jaramillo, J.; Gomperts, R.; Stratmann, R. E.; Yazyev, O.; Austin, A. J.; Cammi, R.; Pomelli, C.; Ochterski, J. W.; Martin, R. L.; Morokuma, K.; Zakrzewski, V. G.; Voth, G. A.; Salvador, P.; Dannenberg, J. J.; Dapprich, S.; Daniels, A. D.; Farkas, Ö.; Foresman, J. B.; Ortiz, J. V.; Cioslowski, J.; Fox, D. J.*Gaussian 09*, revision D.01; Gaussian, Inc.: Wallingford, CT, 2009.
(53) Phillips, J. C.; Braun, R.; Wang, W.; Gumbart, J.; Tajkhorshid, E.; Villa, E.; Chipot, C.; Skeel, R. D.; Kale, L.; Schulten, K. Scalable molecular dynamics with NAMD. *J. Comput. Chem.* **2005**, *26*, 1781−1802.
(54) Ballesteros, J. A.; Weinstein, H. Integrated methods for the construction of three-dimensional models and computational probing of structure-function relations in G protein-coupled receptors. *Methods Neurosci.* **1995**, *25*, 366−428.

DOI: 10.1021/acs.jmedchem.7b01062
J. Med. Chem. 2017, 60, 9641−9652